Proceedings of OMAE'02
21st International Conference on Offshore Mechanics and Arctic Engineering
June 23-28, 2002,Oslo, Norway

OMAE2002-28266

A NUMERICAL TREATMENT OF THE BOUNDARY CONDITIONS FOR STABLE ASSESSMENT OF HYDRODYNAMIC IMPACT PRESSURE

Liang-Yee Cheng
Dept. of Civil Construction Engineering,
Escola Politécnica, University of São Paulo
cheng@pcc.usp.br

Makoto Arai
Faculty of Engineering,
Yokohama National University
m-arai@ynu.ac.jp

ABSTRACT

One of the critical points in the numerical assessment of hydrodynamic impact loads is accurate and stable descriptions of the pressures. Due to discrete approximations adopted by available numerical methods, unnatural violently-oscillating time histories of the impulsive pressure, caused by unstable or even non-converging numerical computation, are generally obtained. The aim of this paper is to investigate the unstable nature of the impulsive pressure computation. Also, a new numerical treatment of the boundary condition for accurate and stable assessment of the sloshing impact pressure based on rectangular grid system is proposed. The comparisons of the computed results with the experimental ones confirmed the accuracy of the proposed technique. The improvements achieved over the existing approaches are also shown herein.

INTRODUCTION

Hydrodynamic impact loads due to slamming on ships navigating in rough seas, wave slapping on offshore structures and sloshing inside liquid cargo tanks are of great concern in the design of ships and offshore structures. Motivated by the development of LNG carriers, VLCCs, moored FPSO systems and increasing size of the liquid cargo tanks associated with the concerns on safety issues, many numerical simulation methods have been proposed in the last decades to predict the hydrodynamic loads caused by severe liquid sloshing. However, accurate and stable assessment of the hydrodynamic impact loads is still one of the most critical points of the numerical approaches [1]. Due to the discrete approximation adopted in almost all the methods, in the discrete space that contains the intersection between the free and rigid boundaries, sudden change of the boundary condition from free surface to rigid one generally occurs. As a result, instead of smoothly-decaying hydrodynamic impact pressure in the real situation, unnatural violently oscillating pressure time histories produced by unstable or even non-converging numerical computation are generally obtained.

Some methods have been proposed to mitigate the instability of the hydrodynamic impact pressure computation. One of the commonly used approaches is setting a buffer layer, on the wall and inside the computational space, where a more gradual transition of the boundary conditions are carried out. However, the results are strongly affected by the numerical parameters of the simulations, such as time step and grid spacing, and their control is a very difficult task. For slamming problems, improvements have been obtained by a method proposed by the authors [2]. It combines body-fitted coordinate system and volume of fluid (VOF) technique. Nevertheless, due to the simple prismatic forms of liquid cargo tanks, a more simple method based on rectangular grids, without using generalized coordinate system, is desirable for the sloshing problems because usually they are more efficient in computation efforts.

The aim of this paper is to investigate the unstable nature of impulsive pressure computation. Also, a numerical treatment of the impact boundary condition for stable and accurate assessment of sloshing impact pressure is proposed. The numerical technique is able to model curved top ceilings by using a rectangular grid system. Two variants of the numerical treatment are discussed and analyzed herein. For the sake of simplicity, all the discussion that follows in this paper will be based on 2D formulations.

Validation of the numerical technique is done by comparing the computed results with the experimental data and published numerical ones. The comparisons confirmed the accuracy of the proposed method and show remarkable improvements made over the existing approaches.

NUMERICAL ISSUES OF IMPULSIVE LOAD ASSESSMENT

When a free surface slams against a rigid boundary, impulsive hydrodynamic loads are produced. After sudden rise up, the impact pressure history at a point decays continuously and smoothly as a consequence of the impulses that are generated without interruption.

However, in the numerical computations, the sudden change of the boundary condition from the free surface to rigid one can not account for continuous nature of the phenomenon due to discrete approximations in time and space. Therefore, impulsive loads associated with the abrupt change of the boundary conditions are detected only at selected points in space and time.

Furthermore, the stability condition for explicit numerical computation

$$\Delta t \le \min\left\{\frac{\Delta x}{|u|}, \frac{\Delta y}{|v|}\right\} \quad , \qquad (1)$$

where,

Δt : time step,

Δx : grid spacing in x (horizontal) direction,

Δy : grid spacing in y (vertical) direction,

u : velocity in x direction,

v : velocity in y direction,

limits the duration of impulse computed at a grid point ($\approx\Delta t$) due to the sudden change to a fraction of the time between slams detected on successive grid points ($\approx\Delta x/|u|$ or $\Delta y/|v|$). In other words, when the hydrodynamic impacts are computed, the numerical duration of collisions between a finite fluid mass and the rigid wall is shorter than the time between successive collisions at the grid points.

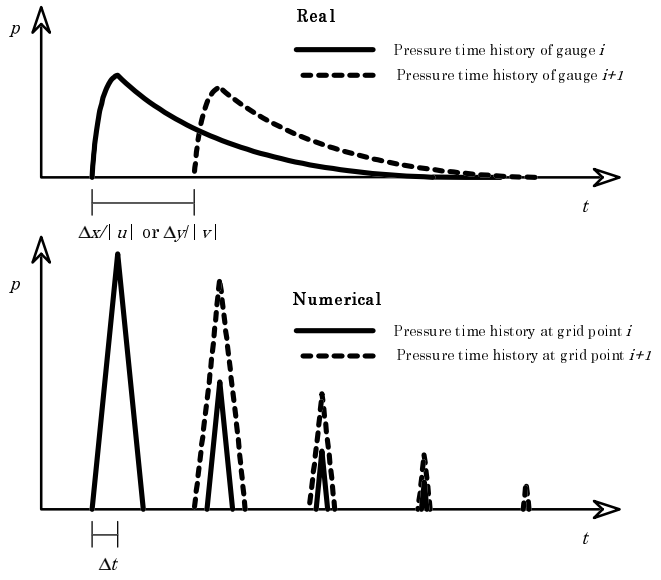

Fig.1 Sketch on behaviors of real and numerical impact pressure.

The factor between the duration of the impulse and the successive slams is approximately equal to $|c_x|=|u|\Delta t/\Delta x$ or $|c_y|=|v|\Delta t/\Delta y$, where c is Courant number and the subscripts x and y indicate the directions. As a consequence, instead of a continuously and smoothly decaying one, numerical solution of the pressure time history consists of a succession of unnatural isolated pulses whose duration seems to be shortened by $|c|$ and the magnitude amplified by $1/|c|$. Figure 1 presents a sketch about this behavior.

The computed impact pressure is very sensitive to the time step. Its magnitude is almost inversely proportional to the value of time step whose inconsistent effect is remarkable: instead of a better result that might be obtained by using a very small time step, a very high maximum value of the pressure and sometimes non-converging computation occurs. However, it is important to point out that, in spite of the shortcoming of the numerical approaches, the impulse associated with the pressure pulses is almost independent to time step.

NUMERICAL TREATMENTS OF THE HYDRODYNAMIC IMPACT BOUNDARY

To overcome the shortcoming of the numerical assessment of the impulsive loads, several approaches have been proposed and investigated. According to a recent survey [3], special treatments for the assessment of impact pressure are adopted by several numerical codes in use. The two main types of the existing treatments are:

- post-treatment of the results by applying an extra pressure, as a function of the velocity, time step and grid spacing, just before the impact and near the impact point,
- inner buffer layer approach, embedded in the numerical computation.

Herein, 'inner buffer layer' means a thin artificial layer set in the fluid domain side of the rigid boundary, between rigid wall and fluid. Inside this thin layer, the transition from free surface to rigid wall may occur gradually, by a linear combination of the free and the rigid boundary conditions as the following expression [4-7]:

$$(1-\kappa)\frac{\Delta y}{\Delta t}(\boldsymbol{v}_f \cdot \boldsymbol{n}_w) + \frac{\kappa(p_s - p_{atm})}{\rho} = 0 \quad , \qquad (2)$$

where,

κ : the weight function for the linear combination,

$\boldsymbol{v}_f$: velocity of the fluid,

$\boldsymbol{n}_w$: normal vector of the rigid wall,

p_s : pressure at the position of the free surface,

p_{atm} : atmospheric pressure,

ρ : density of the fluid,

and

$$\kappa = \begin{cases} \dfrac{\varsigma}{\delta B} & for \quad 0 < \varsigma < \delta B, \\ 0 & for \quad \varsigma \le 0, \\ 1 & for \quad \varsigma \ge \delta B. \end{cases}$$

where,

ζ : distance between free surface and rigid wall,

δB : thickness of the inner buffer layer.

Assuming a very small Δt that satisfies the Eq. (1) is used, the distance ζ^m at the time level m when the transition of the boundary conditions starts can be considered as equal to δB, then the distance ζ^n at a time level n is simplified to

$$\zeta^n = \delta B - \sum_{l=m}^{n} v^l \Delta t \quad . \tag{3}$$

Since δB may be expressed as a fraction of grid spacing

$$\delta B = \frac{\Delta y}{\alpha}, \tag{4}$$

thus, the first expression of the weight function can be rewritten as

$$\kappa^n = 1 - \alpha \sum_{l=m}^{n} c_y^l \quad . \qquad for \qquad 0 < \zeta < \delta B \,, \tag{5}$$

The superscripts l, m and n are used in the equations to designate the time level, where

m : the time level when the transition of the boundary conditions starts,

n : the present time level,

and

v : the velocity of the fluid in y direction,

α : a constant,

c_y : Courant number in y direction, $c_y = v\Delta t/\Delta y$.

The cushioning effect obtained by this treatment attempts to simulate the intermitted states of a boundary cell from empty (free surface) to full (rigid wall) that occur physically. Numerically, this special treatment artificially increases the duration of the impulse computed at a grid point, that is limited by the stability condition.

By applying the inner buffer layer, owing to less violent starts that begin from quasi hydrostatic pressure, the rise up and decay of the localized pressure pulses are moderated. When the thickness of the buffer layer increases, the tendency is to generate a pressure pulses with lower peak value and longer duration. If the duration is longer than the time between slams at successive grid points, the pulses will overlap partially in the time domain. In this way, a smoother pressure time history might be obtained in place of a series of violent isolated spike.

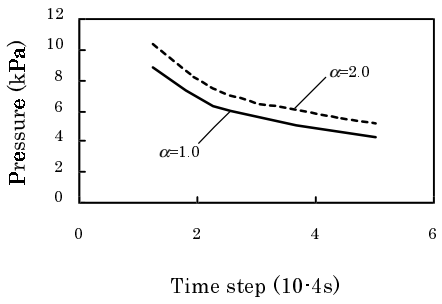

Fig.2 Typical results of the pressure computed on ceiling (12.5mm from the corner) as function of time step (800x400 mm tank, *h/H*=60%, horizontal harmonic excitation *A*=10 mm, *T*=1.1797 s, 160x80 grid)

In spite of the improvement achieved by the application of the inner buffer layer, it still presents several shortcomings that limit this method as a practical one to assess the hydrodynamic pressure. They are:

- dependence of the magnitude of the impact pressure on time step and
- restrictions on the setting of inner buffer layer.

Dependence of the Magnitude of Impact pressure on Time Step

A typical relation between the computed peak value of the impact pressure and the time step used in the numerical computation is shown in Fig. 2.

The calculations were performed by using a rectangular tank whose length (*L*) by height (*H*) is 800x400 mm. The filling (*h/H*) is 60%, where, *h* is the height of the free surface. The forced excitation is a horizontal harmonic motion with amplitude *(A)* of 10 mm and period (*T*) of 1.797 s.

The graph shows that the approach is still inconsistent regarding the numerical parameters because the reduction of time step often produces worse results. Actually, better results might be obtained by reducing the grid spacing and augmenting the time step, but these countermeasures might not be allowed due to the numerical stability issues of the Eq. (1).

Different set of grid size and time step gives very different prediction of pressure pulse, so that it is hard to get a precise and unique description of the impact pressure. However, since the increase of pressure peak is associated with more violent oscillation of the pressure time history when reducing the time step, it may be expected that a stable technique to assess the impact pressure might also eliminate the dependencies of the pressure to the time step.

Restrictions on the Setting of Inner Buffer Layer

Even though there are no more isolated pressure spikes that are brought about by the discrete grid system, it is still difficult to control the unnatural oscillating behavior of the pressure time histories. Thicker inner buffer layer produces better results but from the theoretical point of view, the thickness of the inner buffer layer should not be larger than the grid spacing, otherwise, the impact will take place on the cells that are not the boundary one.

In practice, the combination of computational parameters that gives good results is not clearly known and the 'tuning up' is done mostly case by case. In addition to this, in cases where the rigid walls, such as inclined ceilings, are located inside the grid system, it might be impossible to set a buffer layer with constant or maximum allowed thickness along the boundary cells.

Also, although the formulation of the boundary condition forces the normal component of the fluid velocity be zero at the top ceiling, nothing guarantees that the fluid will reach and stop exactly at the rigid boundary. Actually, thicker the buffer layer and lower the normal velocity, the free surface will stops far

under the top ceiling. On the other hand, with a thinner buffer layer associated with very high velocity component, the free surface may seldom reaches the top ceiling before the velocity component becomes zero. Considering the transition of the boundary condition from free surface to wall as assigning a limited flexibility to the rigid boundary, the position where the free surface stops may be viewed as the displacement of the rigid boundary caused by the hydrodynamic impact. According to this point of view, the behavior of the inner buffer layer is unnatural one because it is expected that the displacement will increase with a larger normal component of the fluid velocity.

A NEW TECHNIQUE FOR THE ASSESSMENT OF THE IMPACT PRESSURE

Based on the above mentioned considerations on the numerical problems and the shortcomings of the approaches using inner buffer layer, a new technique is proposed herein with two improvements on the treatment of the boundary condition:

- the setting of an outer transition region and
- a new weight function to compute the impulsive pressure.

Due to the limitations of the concept based on inner buffer layer to get an adequate thickness, the transition region was set in the outside of the fluid region, that means, the change from the free to rigid boundary starts at the moment when the free surface reaches to the wall. Figure 3 shows the configuration of the outer transition region.

The main advantage of the transition region is that its thickness is automatically adjustable. There is no more limitation due to the grid space, and the thickness might be set as the actual distance need to vanish the normal component of the relative velocity between the fluid and the rigid wall. The distance depends on the velocity component and the parameters of the numerical computation. It varies locally and timely. Lower the normal component of the velocity, a thinner transition region is needed.

As discussed in the section 2, the oscillating behavior of the impact pressure history is caused by the application of the stability condition (Eq.(1)), which reduces the duration of the impulse by a factor approximately equals to the absolute value of Courant number |c| and amplifies numerically the magnitude of the impulse approximately by 1/|c|. In this way, a means to obtain a stable assessment of the pressure is the compensation of the numerical distortion by introducing a factor of |c| in Eq. (2).

In the technique proposed herein, instead of simply multiplying the hydrodynamic pressure term of Eq. (2) by |c|, the weight function of the linear combination between the two boundary conditions was reformulated to include this factor. This is because, as mentioned in section 3 and shown in Eq. (5), the application of the weight function that accounts for the transition of the boundary conditions has already the effect of increasing artificially the duration of the impulse.

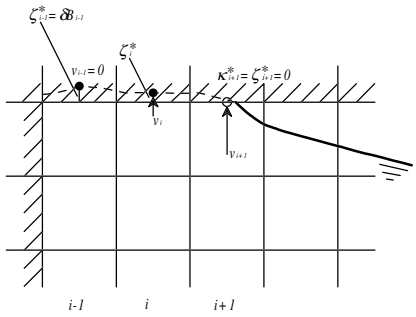

Fig.3 Outer transition region.

The following expressions were proposed.

At first, the Eq. (2) was rewritten as

$$\kappa^* \frac{\Delta y}{\Delta t}(v_f \cdot n_w) + \frac{(1-\kappa^*)(p_s - p_{atm})}{\rho} = 0 \quad . \quad (6)$$

If the same assumption adopted by inner buffer layer is used, the distance ζ^{*n} at time $n\Delta t$ for the outer transition region may be defined as (see Fig. 3)

$$\zeta^{*n} = \sum_{l=m}^{n} v^l \Delta t \quad , \quad (7)$$

Considering that the Courant number c is a function of time and location, there are some possibilities of carrying out the compensation by using different values of c. One of the possibilities is using c^m_y, the local y direction Courant number at the time level m when the impact starts, that yields to:

$$\kappa^{*n} = \kappa_1^{\ *} = \alpha \cdot \left| c_y^m \right| \cdot \sum_{l=m}^{n} (c_y^l) \quad . \quad (8)$$

At the transition, another possibility is to use c^n_y, the local y direction Courant number at present time level n, that results in:

$$\kappa^{*n} = \kappa_2^{\ *} = \alpha \cdot \left| c_y^n \right| \cdot \sum_{l=m}^{n} (c_y^l) \quad . \quad (9)$$

Since the normal component of velocity decreases during the impact, the local y direction Courant number monotonically decreases with time. Thus, we have $\kappa^*_1 \geq \kappa^*_2$. Actually the effects of the compensation due to κ^*_1 is fairly small and higher pressure peaks, associated with the unnatural oscillations of pressure histories are often obtained. Thus, it will not be considered in the validations shown in section 5.

An intermediate formulation between Eq. (8) and (9) may also be defined, as shown in Eq. (10). Here, the $|c^l_y|$ computed timely at the boundary cell was introduced into the summation term of Eq. (5):

$$\kappa^{*n} = \kappa_3^{\ *} = \alpha \sum_{l=m}^{n} \left| c_y^l \right| \cdot (c_y^l) \quad . \quad (10)$$

In the above equations, Courant numbers in y direction c_y are used in the compensation because the change of the boundary conditions is accounted by the fluid motion in the direction y, against the top ceiling.

Detailed descriptions on the other basic issues of the numerical method that were used can be found in references [6] and [7].

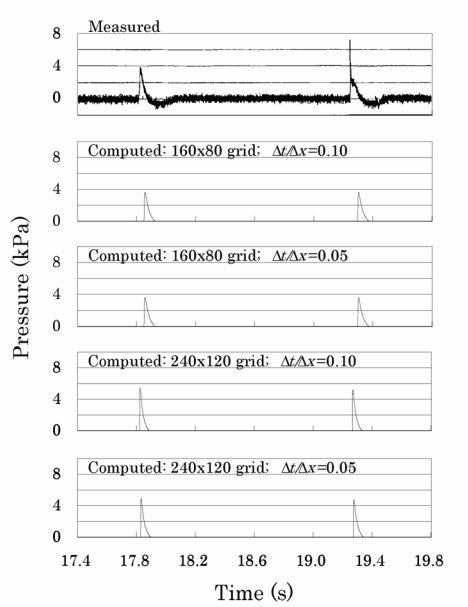

Fig.4 Computed and measured time histories of the impact pressure on the ceiling, 40 mm from the corner (Case A, 1200x600 mm tank, h/H=60%, horizontal harmonic excitation A=15 mm, T=1.47 s, $\kappa^*=\kappa^*_3$).

VALIDATION

Aiming to validate the proposed numerical treatment of the impact boundary conditions, we applied it to simulate numerically several cases of liquid sloshing that were investigated experimentally.

The model tank used for this purpose is a rectangular shaped one and has dimensions L x H of 1200x600 mm. The results of three cases are presented herein:

- Case A: 60% filling with horizontal harmonic motion of 15mm at period of 1.47s,
- Case B: 85% filling with harmonic rolling motion of 8 degrees at period of 1.57s. The center of the rotation coincides with the geometric center of the tank.
- Case C: 45% filling with harmonic rolling motion of 10 degrees at period of 1.71s. The center of the rotation coincides with the geometric center of the tank.

Figure 4 shows the computed pressure time histories on the top ceiling at 40 mm from the corner and the measured one for the case A. The weight function $\kappa^*=\kappa^*_3$ of Eq. (10) was used. Time histories were obtained by using 4 different combinations of time step Δt and grid spacing $\Delta x(=\Delta y)$. The coefficient α used in the computation was set as α=1.0. The magnitude of the pressure increases slightly when reducing Δx but both the magnitude and the duration of the pressure pulses agrees well with the experimental data. After the abrupt rise up, the pressure decays smoothly and continuously, which reflects a considerably stable computation of the impulsive pressure.

A series of calculations for up to 3 values of Δt and values of Δx ranging from $L/\Delta x$=30 to 240 were carried out to investigate the effects of the parameters used in the numerical computation. The results obtained for case A are summarized in Fig. 5. In the figure, the curves link the cases with the same $\Delta t/\Delta x$. Figure 5a shows the result obtained by using $\kappa^*=\kappa^*_2$ (Eq. (9)) and Fig. 5b shows the result obtained by using $\kappa^*=\kappa^*_3$ (Eq. (10)).

According to Fig. 5, the magnitude of the computed impact pressure in the upper left corner reduces with the use of coarse grids. The curves converge asymptotically to constant values as Δx tends to zero. This tendency is reasonable because if we use coarse grids, spatial averaging of the velocity takes effect and might result in a lower magnitude of the impact pressure.

Also, Fig. 5 confirmed a fact suggested by Fig. 4: the computed magnitude of impact pressure is almost independent of time step Δt. This consistent result is of great importance to practical use because an adequate time step Δt, that satisfies numerical stability conditions and other considerations, is sufficient to compute the impact pressure. There is no necessity of further reducing the time step since the results will almost be the same. In other words, the most convenient time step can always be applied to save the processing time because all the concerns about the sensible variation of the pressure magnitude and controls of the unnatural oscillations are eliminated. From Fig. 5a and Fig. 5b, there are almost no difference between the results obtained from $\kappa^*=\kappa^*_2$ (Eq.(9)) and $\kappa^*=\kappa^*_3$ (Eq. (10)), except that the effect of time step is smaller when Eq. (9) is used and, as one may expect, Eq. (9) gives a slightly lower prediction of the impact pressure than Eq. (10) because $|c_y|$ is monotonically decreasing during the impact and $\kappa^*_3 \geq \kappa^*_2$.

The same tendency can be observed in Fig. 6a and Fig. 6b, where the results of the series of calculations for case B are presented. In the figure, the curves link the cases with the same $\Delta t/\Delta x$. Figure 6a shows the results obtained by using $\kappa^*=\kappa^*_2$ (Eq. (9)) and Fig. 6b shows the results obtained by using $\kappa^*=\kappa^*_3$ (Eq. (10)).

However, according to the results shown in Fig. 7, for case C, the difference between the pressures computed by the two weight functions becomes remarkable. The weight function $\kappa^*=\kappa^*_2$ (Eq. (9)) gives much lower prediction of impact pressure than $\kappa^*=\kappa^*_3$ (Eq. (10)), mainly when finer grids are utilized, it is also less susceptible to the change of time step (Fig. 7a). This is because in case C, the resonant motion of 45% filling liquid produces standing wave that hits violently only a small region of the tank's ceiling. Under this severe condition for the pressure computation, the results of $\kappa^*=\kappa^*_3$ (Eq. (10)), that tend to be higher, become unstable for $\Delta t/\Delta x$=0.1. The instability may be confirmed by the effect of time step on the computed pressure: pressure histories with significantly lower peaks and smoother decays are obtained when time step is decreased to $\Delta t/\Delta x$=0.05 (Fig. 7b).

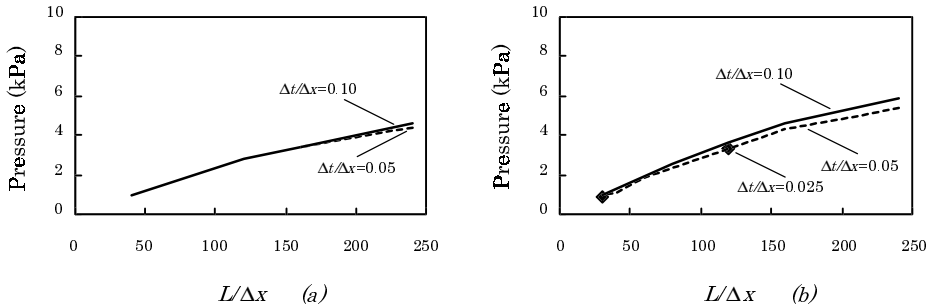

Fig.5 Effects of the grid spacing and time step on the magnitude of impact pressure computed at the upper left corner of the tank: (a) $\kappa^*=\kappa^*_2$; (b) $\kappa^*=\kappa^*_3$ (Case A, 1200x600 mm tank, *h/H*=60%, horizontal harmonic excitation *A*=15 mm, *T*=1.47 s).

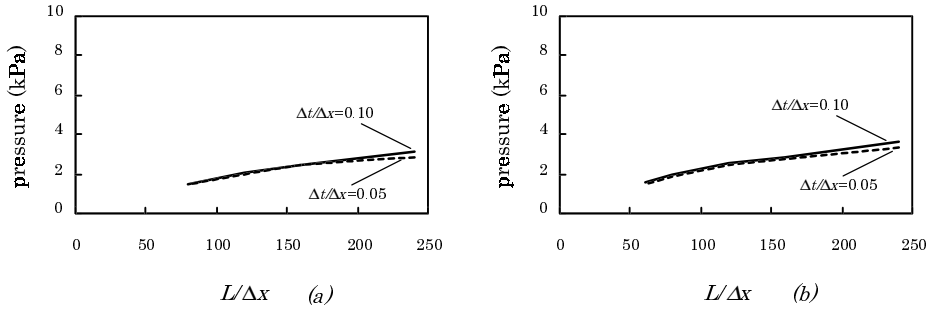

Fig.6 Effects of the grid spacing and time step on the magnitude of impact pressure computed at the upper left corner of the tank: (a) $\kappa^*=\kappa^*_2$; (b) $\kappa^*=\kappa^*_3$ (Case B, 1200x600 mm tank, *h/H*=85%, harmonic rolling excitation $\theta=8^O$, *T*=1.57 s).

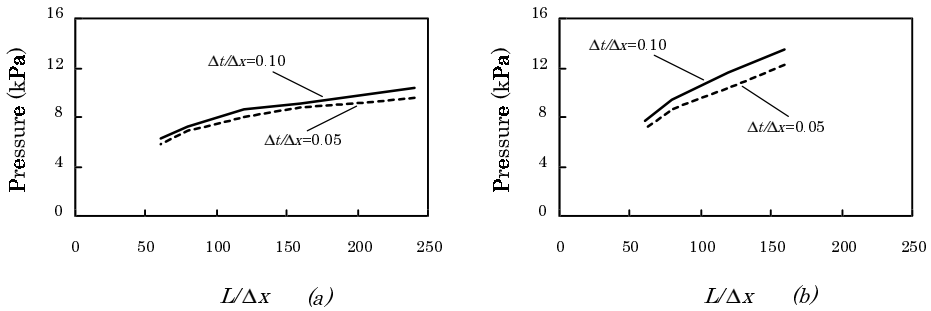

Fig.7 Effects of the grid spacing and time step on the magnitude of impact pressure computed at the upper left corner of the tank: (a) $\kappa^*=\kappa^*_2$; (b) $\kappa^*=\kappa^*_3$ (Case C, 1200x600 mm tank, *h/H*=45%, harmonic rolling excitation $\theta=10^O$, *T*=1.71 s).

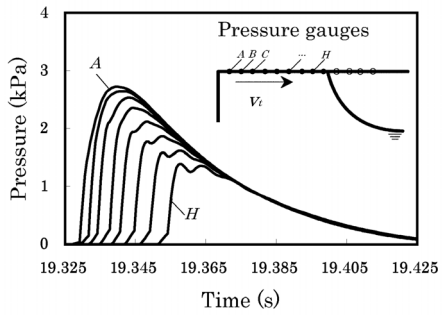

Fig.8 Pressures computed at the boundary grids (Case A, 1200x600 mm tank, *h/H*=60%, horizontal harmonic excitation *A*=15 mm, *T*=1.47 s, 120x60 grid, Δ*t*=0.0005 s, $\kappa^*=\kappa^*_2$).

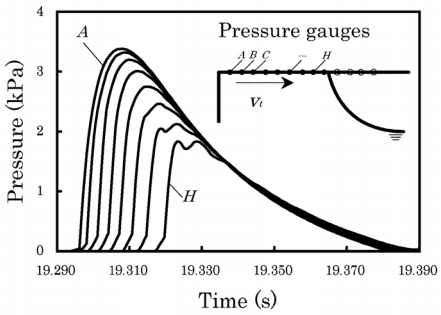

Fig.9 Pressures computed at the boundary grids (Case A, 1200x600 mm tank, *h/H*=60%, horizontal harmonic excitation *A*=15 mm, *T*=1.47 s, 120x60 grid, Δ*t*=0.0005 s, $\kappa^*=\kappa^*_3$).

Figure 8 presents a sequence of pressure time histories in the positions *A* to *H* of the top ceiling, computed by using $\kappa^*=\kappa^*_2$ (Eq. (9)) for case A. The distances of the positions *A, B, C*, etc. to the corner are 5 mm, 15 mm, 25 mm and so on. It is clear that the continuous and smooth decaying pressure curves can be obtained for nearly all the region of impact. In the last boundary cells where the impact occurs, slight oscillation of the computed pressure might be observed. The reason seems to be non-overlapping isolated pulses generated at these cells when few or no subsequent pulses exists.

The results of the calculation carried out by using $\kappa^*=\kappa^*_3$ (Eq. (10)) is given in Fig. 9. Except a slightly higher pressure peak, and a small shift in the phase, the behavior of the pressure histories is almost equal to that of Fig. 8.

The influences of the constant α used in the weight functions have been analyzed together with the verification of the accuracy of the present numerical treatment.

Figure 10 was obtained from a series calculation carried out with the model tank in case A. Both weight functions $\kappa^*=\kappa^*_2$ (Eq. (9)) and $\kappa^*=\kappa^*_3$ (Eq. (10)) were used. All the calculations were performed with $\Delta t/\Delta x$=0.1. The curves in the graph show the impact pressure at upper left corner as functions of the grid spacing, parameterized by the coefficient α. The tendencies observed in Fig. 4 are again confirmed herein. Also, from the graph, it represents clearly that the use of a larger coefficient α increases the computed pressure peak. Comparing the curve of α=1.0, we may conclude that the weight function , $\kappa^*=\kappa^*_2$ (Eq. (9)) gives a slightly underestimated prediction of about 80% the value that is obtained by $\kappa^*=\kappa^*_3$ (Eq. (10)).

Since the measured maximum peak values of the impact pressure present some scatterings, histogram of the measured values on the top ceiling at 40 mm from the corner is given in the right side of the graph. The histogram indicates that about 75% of the measured values fall into 3.0 to 6.0 kPa, with the maximum frequency (22.0%) at about 5.0 kPa, which is within the range of the result obtained by using α=1.0 to 2.0, for $\kappa^*=\kappa^*_2$, and α=1.0, for $\kappa^*=\kappa^*_3$, combined with a fine grid with 120x60 to 240x120 cells. When using larger α, such as α=4.0 for $\kappa^*=\kappa^*_3$, a coarse grid of 60x30 to 80x40 is sufficient to obtain the desired result, however, in this case, the use of a finer grid leads to an overestimated value.

Similar results were obtained for the cases B. As illustrated in Fig. 11, about 75% of the measured maximum peak values are within the range of 2.0 to 5.0 kPa, with the maximum frequency (28.5%) at about 3.0 kPa, which corresponds approximately to the results obtained by using α=1.0 to 2.0, for $\kappa^*=\kappa^*_2$, and α=1.0, for $\kappa^*=\kappa^*_3$, combined with a fine grid with 120x60 to 240x120 cells. As in case A, use of larger α, such as α=4.0 for $\kappa^*=\kappa^*_3$, together with a coarse grid of 60x30 or 80x40 is sufficient to obtain a similar result. As may be expected, in this case the weight function $\kappa^*=\kappa^*_2$ (Eq. (9)) also gives slightly lower predictions than the results when using $\kappa^*=\kappa^*_3$ (Eq. (10)).

Figure 12 gives the results for the case C. In this case, very violent liquid motion occurs and, since the standing wave hits severely only a small region of the tank's ceiling, it may be considered a case extremely difficult to be simulated. The histogram of the Fig. 12 shows that the measured impact pressure peaks are widely spreading, ranging from 2 kPa to 25 kPa. About 85% of the measured maximum peak values are within the range of 2.5 to 12.5 kPa, which corresponds approximately to the result obtained by using α=1.0 to 2.0, for $\kappa^*=\kappa^*_2$, combined with a fine grid with 120x60 to 240x120 cells. Even under the severe condition, the weight function $\kappa^*=\kappa^*_2$ (Eq. (9)) leads to stable pressure computations. However, since the maximum frequency (27.1%) is at about 5.0 kPa and the mean at about 7.5 kPa, it seems that, in spite of the stable computations, the results are slightly overestimated in this case. On the other hand, as mentioned before in Fig. 7, the weight function $\kappa^*=\kappa^*_3$ (Eq. 10) results in a significant overestimated pressure for α lager the 2.0 in the whole range of grid spacing because oscillation of the pressure history already occurs.

Figure 13 gives the relation between the computed impact pressure at the upper left corner and the coefficient α. Grid with 160x80 cells was used in these calculations. The graph is parameterized with constant $\Delta t/\Delta x$ curves, that shows the effect of change in time step Δt. Figure 13a corresponds to case A and Fig. 13b corresponds to case B. The results indicate that the effect of the time step is negligible when the coefficient α is small, such as α=0.5 and 1.0. However, when α increases, such as α=4.0, it influences on the computed pressure increases remarkably. Also in such case the computed impact pressure tends to present oscillating behaviors.

In the extreme case of using $\alpha=1/|c|$, the compensation for Courant number no more exists: considering the difference due to the transitions in the inner and outer side of fluid domain, that are expressed by the Eq. (3) and Eq. (7), respectively, when $\alpha=1/|c|$, the weight function κ^* (Eq. (9) or Eq. (10)) becomes similar to κ (Eq. 5). This means unnatural oscillating results of the pressure computation will be obtained. Therefore, for practical applications, coefficient α ranging from 1.0 to 2.0 should be used.

From the above results, it becomes clear that the effect of time step on the magnitude of the pressure peak reflects the instability, i.e., the unnatural oscillating behavior of the impulsive pressure, of the calculation. Therefore, the sensibility of the computed pressure to the variation of time step may be used as a method to check the stability of the pressure computation.

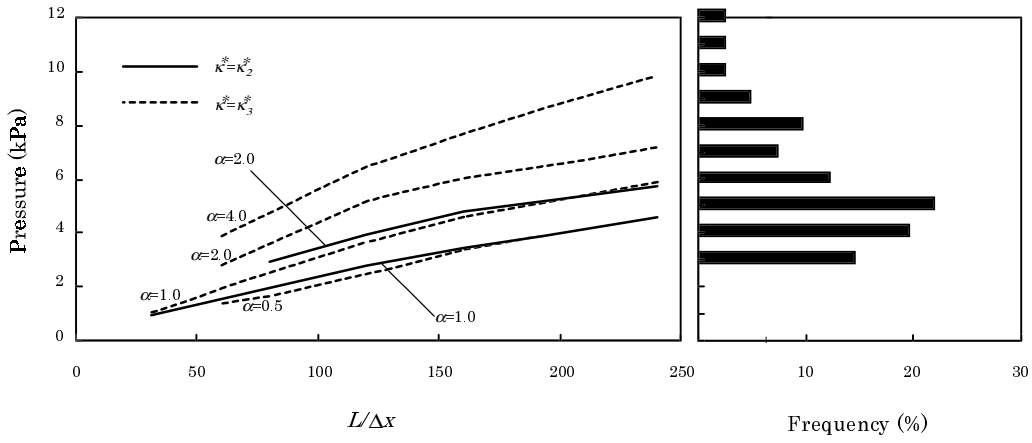

Fig.10 Effects of the coefficient α on the magnitude of impact pressure computed at the upper left corner of the tank and the histogram of the measured pressure (Case A, 1200x600 mm tank, *h/H*=60%, horizontal harmonic excitation *A*=15 mm, *T*=1.47 s).

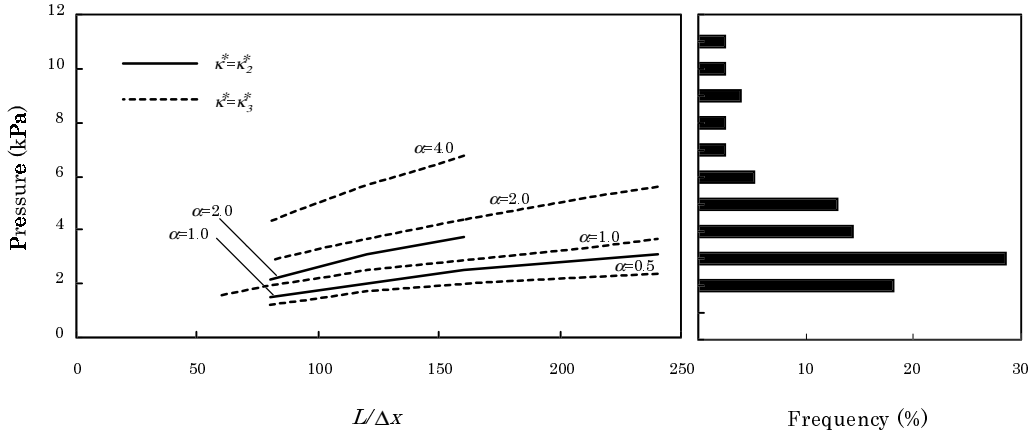

Fig.11 Effects of the coefficient α on the magnitude of impact pressure computed at the upper left corner of the tank and the histogram of the measured pressure (Case B, 1200x600 mm tank, *h/H*=85%, harmonic rolling excitation θ=8^O, *T*=1.57 s).

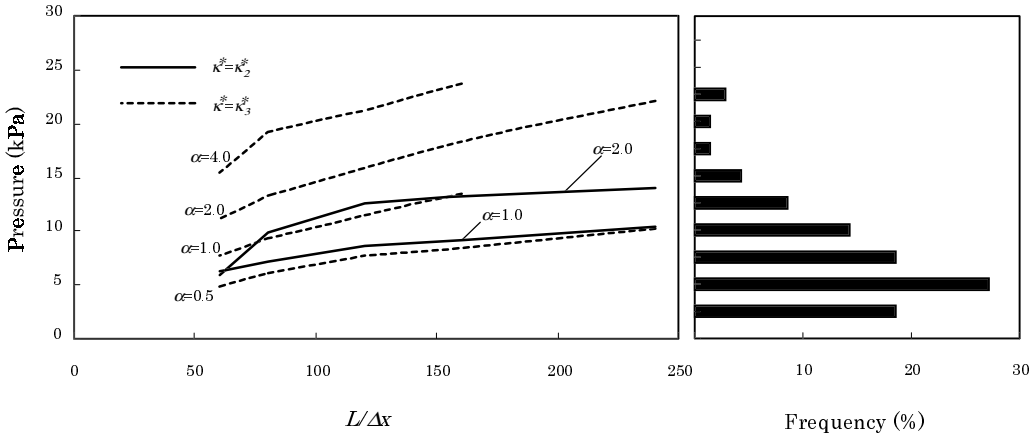

Fig.12 Effects of the coefficient α on the magnitude of impact pressure computed at the upper left corner of the tank and the histogram of the measured pressure (Case C, 1200x600 mm tank, *h/H*=45%, harmonic rolling excitation θ=10^O, *T*=1.57 s).

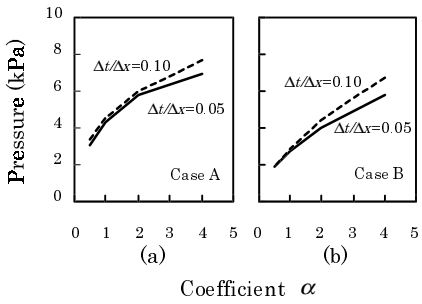

Fig.13 Effects of the coefficient α on the impact pressure computed at the upper left corner of the tank (Cases A and B, 160x80 grid, $\kappa^*=\kappa^*_3$).

Finally, to give a better insight of the improvements achieved by the present technique upon the existing ones, a comparison of the pressure time histories between the present numerical technique and other researcher's results [3] is shown in Fig. 14. It is a 2D computation on a rectangular model tank sized 800x400 mm with 60% filling. The excitation is horizontal harmonic motion of 10 mm at period of 1.1797 s. $\kappa^*=\kappa^*_3$ (Eq. (10)) was used in the calculations. In the right side of Fig. 14, there are the pressure plots obtained by the 11 numerical codes that participated in the test. According to Cariou and Casella [3], these codes could be considered as represents of the states of the art of the numerical methods for liquid sloshing. The pressure probe is located on the left wall at 80 mm height, which is quite far from the impact region on the top ceiling of the tank. However, even in this situation, all of the 11 pressure plots present oscillations that are typical ones due to unstable impulsive pressure computed on the top ceiling.

The left hand side of the Fig. 14 gives computed results of the present technique. Instead of oscillating pressure plots, very smooth ones have been obtained without any kind of averaging technique or any other post treatment for the computed impact pressure. Due to the stable computation of the impulsive pressures on the top ceiling achieved by the technique, no undesirable influences have been transmitted to the pressure probe located near the bottom. The computation were carried out with 80x40 grid and time step of 0.001 s.

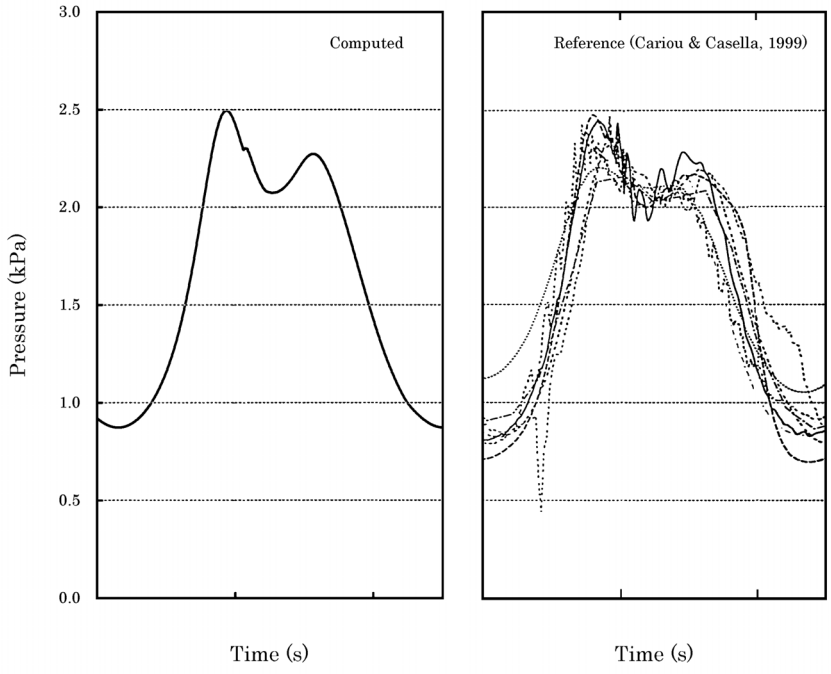

Fig.14 Improvement of the numerical technique over the exiting ones (800x400 mm tank, h/H=60%, horizontal harmonic excitation A=10 mm, T=1.1797S, 80x40 grid, Δt=0.001 s, $\kappa^*=\kappa^*_3$).

CONCLUDING REMARKS

Correct prediction of hydrodynamic impact loads is one of topics remained in the numerical study of the liquid sloshing. Since most of the liquid cargo tanks have simple prismatic forms, a numerical treatment of the impact conditions that gives stable and accurate impact pressure computation is desired. In the present paper, the mechanism of the unstable impulsive pressure computation is discussed and a new technique for stable assessment of hydrodynamic impact pressure in sloshing simulation is presented. By introducing a stabilization factor $|c|$ on the control of the transition from free to rigid boundaries, the numerical method produces consistent behaviors regarding the variation of the numerical parameters and very smooth and natural impulsive pressure time histories are obtained.

The results of the validation show that, beside very stable computations obtained without using complex generalized coordinate systems, or post treatment techniques, the magnitude and the form of the impact pressure on the tank ceiling are in excellent accordance with the experimental ones. What is more, unlike the traditional approaches, the magnitude of the computed impact pressure is almost independent to the numerical parameters such as time step. For finer grids, more accurate impact pressures are obtained while in the case of coarse grids, due to the local averaging effect, lower impact pressure are computed.

The effects of the constant α used in the weight functions were analyzed together with the verification of accuracy. The results indicate that for practical applications, weight function given in Eq. (9) and coefficient α ranging from 1.0 to 2.0 should be used.

Concerning the design practice, research is still necessary to investigate the actual effects of the impulsive loads on structural response. However, undoubtedly, the stable pressure assessment achieved by the present numerical technique will contribute to the further studies.

ACKNOWLEDGMENTS

The author would like to express their gratitude to Mr. Atsushi Kumano of ClassNK and Mr. Takeshi Miyamoto of National Maritime Research Institute, Japan, for their cooperation in conducting the model experiments.

REFERENCES

[1] Committee 1.2. “Loads” – Report, 13th ISSC 1997, vol. 1.

[2] Arai, M., Cheng, L. Y, Inoue, Y. : A Computing Method for the Analysis of Water Impact of Arbitrary Shaped Bodies, Journal of the Society of Naval Architects of Japan, Vol. 176 (1994), pp.233-240.

[3] Cariou, A., Casella, G. : Liquid Sloshing in Ship Tanks: a Comparative Study of Numerical Simulation, Marine Structure Journal, 12, 1999, pp. 183-198

[4] Hirt, C. W., Nichols, B. D., Romero, N. C. : SOLA – A Numerical Solution Algorithm for Transient Fluid Flows, Los Alamos Scientific Laboratory, Report LA-5852 (1975).

[5] Belytschko, T., Mullen, R. : Two Dimensional Fluid-Structure Impact Computations, ASME, 80-C2/PVP-139 (1980).

[6] Arai, M. : Experimental and Numerical Studies of Sloshing Pressure in Liquid Cargo Tanks, Journal of the Society of Naval Architects of Japan, Vol. 155 (1984), pp.121-127.

[7] Arai, M., Cheng, L. Y, Inoue, Y. : 3D Numerical Simulation of Impact Loads due to Liquid Cargo Sloshing, Journal of the Society of Naval Architects of Japan, Vol. 171 (1992), pp.317-324.